

Constrained sinogram restoration for limited-angle tomography

Jerry L. Prince

The Johns Hopkins University
Department of Electrical
and Computer Engineering
Image Analysis and Communications
Laboratory
105 Barton Hall
Baltimore, Maryland 21218

Alan S. Willsky

Massachusetts Institute of Technology
Department of Electrical Engineering
and Computer Science
Laboratory for Information and Decision
Systems
Room 35-437
Cambridge, Massachusetts 02139

Abstract. Tomographic reconstruction from incomplete data is required in many fields, including medical imaging, sonar, and radar. In this paper, we present a new reconstruction algorithm for limited-angle tomography, a problem that occurs when projections are missing over a range of angles. The approach uses a variational formulation that incorporates the Ludwig-Helgason consistency conditions, measurement noise statistics, and a sinogram smoothness condition. Optimal restored sinograms, therefore, satisfy an associated Euler-Lagrange partial differential equation, which we solve on a lattice using a primal-dual optimization procedure. Object estimates are then reconstructed using convolution backprojection applied to the restored sinogram. We present results of simulations that illustrate the performance of the algorithm and discuss directions for further research.

Subject terms: image reconstruction; computed tomography; regularization; limited-angle tomography; primal-dual optimization.

Optical Engineering 29(5), 535-544 (May 1990).

CONTENTS

1. Introduction
2. Limited-angle tomography
3. Sinogram restoration approach
 - 3.1. Variational formulation
 - 3.2. Euler-Lagrange equations
 - 3.3. Initial estimate of Lagrange multipliers
 - 3.4. Primal-dual restoration algorithm
4. Results
5. Discussion
6. Acknowledgments
7. Appendixes
 - 7.1. Derivation of equilibrium partial differential equation
 - 7.2. Indexing the basis functions
 - 7.3. Lagrange multiplier approximation
 - 7.4. Local relaxation algorithm
8. References

1. INTRODUCTION

Limited-angle tomography is a problem that arises in a number of applications, including medical imaging, sonar, radar, non-destructive evaluation, geophysical exploration, and hologra-

phy. The aim is to reconstruct a function defined on the plane from a set of (possibly noisy) one-dimensional projections that are available over an angular range less than the ideal 180°. It is an inverse problem that is inherently ill conditioned and yet is so important in so many applications that it has received considerable attention over the past 10 years. The main conclusion to be drawn from this body of literature is that correct prior knowledge—possibly quite particular to the given problem—and optimal use of known noise statistics are the keys to obtaining adequate reconstructions.

In this paper we present an algorithm that restores a complete sinogram, which can then be used to reconstruct an object using ordinary convolution backprojection. The restored sinogram is the solution of a variational formulation that incorporates the Ludwig-Helgason consistency conditions,^{1,2} known noise statistics, and a smoothness property of sinograms, which constitutes our prior knowledge. Thus, restored sinograms are consistent in the sense that they are in the range of the 2-D Radon transform operator, they optimally balance prior knowledge with noisy observations (in a maximum a posteriori sense), and they reflect our prior knowledge of smoothness.

This research complements and advances research related to limited-angle tomography that we have previously reported.³⁻⁵ In two of these works^{3,4} we describe methods to estimate an object's convex support from collections of noisy support line

Invited Paper RR-114 received Oct. 29, 1989; revised manuscript received Jan. 2, 1990; accepted for publication Jan. 3, 1990.
© 1990 Society of Photo-Optical Instrumentation Engineers.

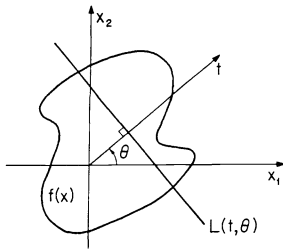


Fig. 1. The geometry of computed tomography.

measurements, information that may be derived from observed projections.⁶ This convex support information is used together with other geometric knowledge in a limited-angle reconstruction approach similar to that which appears in this paper.⁵ However, this previous work includes only two constraints, mass and center of mass, and requires that these be known a priori. The current work incorporates a (theoretically) infinite number of consistency constraints without requiring any prior knowledge related to consistency.

This paper is organized as follows: In Sec. 2 we review the limited-angle tomography problem and discuss important past contributions. In Sec. 3 we develop and state our sinogram restoration algorithm. This includes a description of the variational principle, its exact solution, and a discussion of the computational methods used to obtain numerical results. In Sec. 4 we present results of simulations that demonstrate the algorithm's performance, and finally we give a brief summary and discussion of future research in Sec. 5.

2. LIMITED-ANGLE TOMOGRAPHY

The geometry of computed tomography is shown in Fig. 1. Here, the function $f(x)$ is integrated along lines $L(t, \theta)$, where t is the lateral displacement of lines orthogonal to the unit vector $\omega = (\cos\theta, \sin\theta)$. A complete parallel-ray projection at angle θ is denoted $g(t, \theta)$, which when thought of as a function of both t and θ is called the 2-D Radon transform of $f(x)$ and is given by

$$g(t, \theta) = \int_{\mathcal{R}^2} f(x) \delta(t - \omega \cdot x) dx \quad (1)$$

A sinogram is created by displaying $g(t, \theta)$ as an image, where we let $0 \leq \theta < \pi$ be the x -axis range and $-1 \leq t \leq 1$ be the y -axis range, which assumes that the object is supported on the unit disk. We denote the domain of a sinogram by

$$\mathcal{Y} = \{(t, \theta) | 0 \leq \theta < \pi, -1 \leq t \leq 1\} \quad (2)$$

Since the 2-D Radon transform is invertible,⁷ when all values of a sinogram are known (and are noise free) then the corresponding object may be reconstructed perfectly and uniquely. For any finite set of measurements there is no unique reconstruction,⁸ however, excellent results are obtained by a variety of methods, including convolution backprojection (CBP), an algebraic reconstruction technique (ART), and the Fourier method, if there are sufficient numbers of samples in t and θ that cover the sinogram domain adequately.⁹ Limited-angle data lack projections over some angular range (or ranges) and produce poor reconstructions that are rife with artifacts if the usual algorithms are applied.

One reason that application of the usual reconstruction techniques to limited-angle data fails is that these approaches do not consider the consistency of the 2-D Radon transform. As an example of lack of consistency, consider a sinogram that has positive values over the range of projections where measurements exist and is zero over the range of missing projections. Such a sinogram is not a valid 2-D Radon transform and, therefore, does not have an inverse. The conditions that describe the consistency of the 2-D Radon transform were first stated by Ludwig,¹ later expanded on by Helgason,² and may be stated for our purposes as follows:

Theorem 1 (2-D Consistency Theorem)—Let \mathcal{S} be the space of rapidly decreasing C^∞ functions on \mathcal{R}^2 and let S^1 be the unit circle. Then, in order for $g(t, \theta)$ to be the 2-D Radon transform of a function $f \in \mathcal{S}$, it is necessary and sufficient that (a) $g \in \mathcal{S}(\mathcal{R}^1 \times S^1)$, (b) $g(t, \theta + \pi) = g(-t, \theta)$, and (c) the integral

$$\int_{-\infty}^{\infty} g(t, \theta) t^k dt \quad (3)$$

be a homogeneous polynomial of degree k in $\cos\theta$ and $\sin\theta$ for all $k \geq 0$. Condition (c) may be replaced by the following condition (d): If $k < l$, then

$$\int_0^{2\pi} \int_{-\infty}^{\infty} g(t, \theta) t^k \frac{1}{\sqrt{\pi}} \cos l \theta dt d\theta = 0 \quad (4)$$

$$\int_0^{2\pi} \int_{-\infty}^{\infty} g(t, \theta) t^k \frac{1}{\sqrt{\pi}} \sin l \theta dt d\theta = 0 \quad (5)$$

Two important geometrical relationships that exist between an object and its 2-D Radon transform follow from direct use of condition (c) in Theorem 1. The first relationship results from setting $k = 0$ in Eq. (3), where it follows that the integral of any projection is a constant. It then follows from Eq. (1) that

$$\mu = \int_{-\infty}^{\infty} g(t, \theta) dt = \int_{\mathcal{R}^2} f(x) dx \quad \forall \theta \quad (6)$$

where the constant μ will be referred to as the mass of $f(x)$. The second relationship follows from setting $k = 1$ in Eq. (3), which leads to

$$c(\theta) = \frac{1}{\mu} \int_{-\infty}^{\infty} t g(t, \theta) dt = \omega \cdot \frac{1}{\mu} \int_{\mathcal{R}^2} x f(x) dx \quad (7)$$

This relationship reveals that the center of mass of the projection at angle θ , i.e., $c(\theta)$, is equal to the projection of the center of mass of the object onto the ω -axis.

Several researchers have directly incorporated the consistency conditions into reconstruction algorithms in the past. Ein-Gal¹⁰ was the first to propose consistency of the sinogram as a reconstruction criterion. Peres,¹¹ Louis and Natterer,^{7,12} and more recently, Saito and Kudo¹³ used variants of Ein-Gal's approach for limited-angle data. These researchers used the fact that in

Eqs. (4) and (5), t^k may be replaced by $P_k(t)$, the normalized Legendre polynomial of degree k , without changing the equality. Then one recognizes that the product $P_k(t)S_{lm}(\theta)$, where $S_{11}(\theta) = (1/\sqrt{\pi})\cos\theta$ and $S_{12}(\theta) = (1/\sqrt{\pi})\sin\theta$, forms a complete orthonormal basis on $\mathcal{R}^1 \times S^1$. Therefore, the coefficients

$$a_{lm}^k = \int_0^{2\pi} \int_{-1}^1 g(t, \theta) P_k(t) S_{lm}(\theta) dt d\theta \quad (8)$$

are generalized the Fourier coefficients of $g(t, \theta)$, which, by condition (d) of theorem 1, are free to be nonzero only when $k \geq l$.

The free Fourier coefficients of Eq. (8) may be estimated by taking the inner product of each available projection with the Legendre polynomials and solving a system of linear equations.^{11,12} The object can then be reconstructed by computing a sufficient number of uniformly spaced projections over $[0, \pi)$ using the estimated generalized Fourier coefficients and applying convolution backprojection, for example. Peres¹¹ points out that the "existence of noise imposes severe limitations on reconstructions from limited angular data," and that one cannot expand to an arbitrarily large number of coefficients without severe degradations of the reconstructions. Louis¹² derives error bounds for noise-free projections and claims that the method is useful "even if the range is only $[0, 2\pi/3]$." It should be emphasized that while these approaches use the consistency conditions, they do not incorporate noise in any optimal sense, nor do they attempt to impose additional prior knowledge.

Other researchers have used the idea of consistency but have avoided explicit expansion of the Radon transform. For example, many approaches iterate between object space and Radon space, imposing known constraints and measurements until the object is consistent with the measurements.¹⁴⁻¹⁷ Ravichandran and Gouldin¹⁸ explicitly restrict the class of reconstructable functions and estimate coefficients of basis functions in the projections that are consistent with that class. By imposing severe smoothness conditions they have been able to obtain good reconstructions from only four (noise-free) projections. Finally, Buonocore proposed a fast minimum variance estimator that is based on an unusual pixel decomposition, and he showed that it satisfies the consistency conditions.¹⁹

Our approach is to restore the partially observed sinogram to one that is complete (in its projections), consistent with the Ludwig-Helgason consistency conditions, that reflects the known noise statistics and is smooth. It is a projection-space approach since we do not iterate in either Fourier space or object space during the restoration process. The unique aspect is the variational formulation on the continuum, which yields an exact solution on the continuum. As revealed below, this formulation provides for the desired properties of restored sinograms and yields an efficient iterative algorithm for numerical solution.

3. SINOGRAM RESTORATION APPROACH

3.1. Variational formulation

Let \mathcal{Y} be the sinogram domain as defined in Eq. (2) and let \mathcal{Y}_o be the subset of \mathcal{Y} over which projection measurements y are available. We define the restored sinogram to be the sinogram g that minimizes

$$I = \iint_{\mathcal{Y}_o} \frac{1}{2\sigma^2} (y - g)^2 dt d\theta + \iint_{\mathcal{Y}} \left[\beta \left(\frac{\partial g}{\partial t} \right)^2 + \gamma \left(\frac{\partial g}{\partial \theta} \right)^2 \right] dt d\theta \quad (9)$$

subject to the equality constraints

$$J_{lm}^k = \int_0^{2\pi} \int_{-1}^1 g(t, \theta) P_k(t) S_{lm}(\theta) dt d\theta = 0 \quad , \quad (10)$$

for $m = 1, 2$ and $k, l = 0, 1, \dots$, where $k < l$. In addition, the boundary conditions

$$\begin{aligned} g(1, \theta) &= g(-1, \theta) = 0 \quad , \\ g(t, 0) &= g(-t, \pi) \quad , \end{aligned} \quad (11)$$

must also be satisfied. Here, β and γ are positive constants, σ^2 is the measurement noise intensity, and $P_k(t)$ are the Legendre polynomials normalized so that

$$\int_{-1}^1 P_j(t) P_k(t) dt = \delta_{jk} \quad , \quad (12)$$

where δ_{jk} is the Kronecker delta function.

The motivation for minimizing I is as follows: The first term keeps the sinogram values close to the measurements but is weighted by the noise intensity so that with large noise intensity this term becomes less important. This term also arises in optimal smoothing solutions for processes observed in white noise with intensity σ^2 (Ref. 20). The second term creates smooth sinograms, where the amount of smoothness in each of the two directions is controlled by parameters β and γ , which must be fixed a priori. This second term may be considered to be a regularizing term or, alternatively, it may be seen to be analogous to the logarithm of a prior probability on sinograms. In fact, in Ref. 5 we show that a particular numerical solution of this type of problem solves a maximum a posteriori (MAP) formulation for the sinogram defined as a particular Markov random field.

The circular harmonics $S_{lm}(\theta)$ as defined in Sec. 2 are orthonormal over the unit circle, and therefore, the product $P_k(t)S_{lm}(\theta)$ forms a complete orthonormal basis over $[-1, 1] \times [0, 2\pi]$. The sinogram domain includes only half of this angular range; therefore, the constraints in Eq. (10) must be restated to correspond to the sinogram domain. To do this, we use the symmetry relation $g(t, \theta + \pi) = g(-t, \theta)$ from Theorem 1 and the fact that $S_{lm}(\theta + \pi) = (-1)^l S_{lm}(\theta)$ and $P_k(-t) = (-1)^k P_k(t)$, to obtain

$$J_{lm}^k = \int_0^\pi \int_{-1}^1 g(t, \theta) S_{lm}(\theta) P_k(t) [1 + (-1)^{k+l}] dt d\theta \quad . \quad (13)$$

Now we see that when $k + l$ is odd in Eq. (13), J_{lm}^k is identically zero, and therefore, it is not necessary to impose these constraints explicitly. Thus, the required constraints to be imposed over the sinogram domain are

$$J_{lm}^k = \int_0^\pi \int_{-1}^1 g(t, \theta) S_{lm}(\theta) P_k(t) dt d\theta = 0 \quad , \quad (14)$$

for $m = 1, 2$ and $k, l = 0, 1, \dots$, where $k < l$ and $k + l$ is even.

3.2. Euler-Lagrange equations

The exact solution of the above variational problem, found using the calculus of variations,²¹ is the Euler-Lagrange equation given by

$$\frac{1}{\sigma^2} \chi_Y g - 2\beta \frac{\partial^2 g}{\partial t^2} - 2\gamma \frac{\partial^2 g}{\partial \theta^2} = \frac{1}{\sigma^2} \chi_Y y - \sum_i \lambda_i \Psi_i, \quad (15)$$

where the index i denotes the triplet $i = (k, l, m)$ of indices, $\Psi_i = P_k(t)S_l m(\theta)$, and χ_Y is the characteristic function of the measurement set \mathcal{Y}_o , equal to one where $(t, \theta) \in \mathcal{Y}_o$ and zero otherwise. The solution must also satisfy the original constraints and boundary conditions in Eqs. (14) and (11) and the additional boundary condition

$$\frac{\partial g(t, 0)}{\partial t} = \frac{\partial g(-t, \pi)}{\partial t}. \quad (16)$$

An outline of the variational methods yielding Eq. (15) appears in Sec. 7.1, and one method to index the basis functions $\{\Psi_j\}$ is given in Sec. 7.2.

We now have that the restored sinogram, which minimizes I , also satisfies the partial differential equation (PDE) in Eq. (15). But this PDE has an infinite number of additional unknowns: the Lagrange multipliers $\{\lambda_i\}$. Truncating the infinite summation to, say, p terms, makes the problem tractable but does not prevent the obvious; that we now must solve simultaneously for the restored sinogram and for a set of Lagrange multipliers.

3.3. Initial estimate of Lagrange multipliers

One can solve for the Lagrange multipliers exactly by multiplying both sides of Eq. (15) by Ψ_j and integrating over the sinogram domain. Using the orthogonality of the basis functions, where it can be shown that when $k + l$ is even, $\iint_{\mathcal{Y}} \Psi_i \Psi_j dt d\theta = \frac{1}{2} \delta_{ij}$, we have

$$\lambda_j = -2 \iint_{\mathcal{Y}} \left[\frac{1}{\sigma^2} \chi_Y g - 2\beta \frac{\partial^2 g}{\partial t^2} - 2\gamma \frac{\partial^2 g}{\partial \theta^2} - \frac{1}{\sigma^2} \chi_Y y \right] \Psi_j dt d\theta, \quad j = 1, \dots, p. \quad (17)$$

As shown in Sec. 7.3, Eq. (17) may be approximated by

$$\lambda_j \approx 2 \iint_{\mathcal{Y}} \frac{1}{\sigma^2} \chi_Y y \Psi_j dt d\theta, \quad j = 1, \dots, p, \quad (18)$$

which is a good approximation when β is small, $f(x)$ is disappearing on its boundary, and χ_Y is 1 on \mathcal{Y} . This approximation allows us to choose starting Lagrange multipliers that are close to the final values, resulting in considerable computational savings.

3.4. Primal-dual restoration algorithm

The primal-dual algorithm described in this section finds both $g(t, \theta)$ (on a discrete set of lattice points) and p Lagrange multipliers $\lambda_1, \lambda_2, \dots, \lambda_p$, which together satisfy Eq. (15). In addition, $g(t, \theta)$ also satisfies the constraints given in Eq. (14) and bound-

ary conditions given by Eqs. (11) and (16). We note that for fixed Lagrange multipliers, the PDE of Eq. (15) may be solved numerically on a discrete lattice system over \mathcal{Y} so that $g(t, \theta)$ will satisfy the boundary conditions—this is the *primal* stage. Then, if $g(t, \theta)$ also happens to satisfy the constraints, we are done. Otherwise, the Lagrange multipliers must be adjusted—this is the *dual* stage—so that another primal iteration may be made. We summarize the algorithm as follows:

Algorithm 1 (Primal-Dual Sinogram Restoration)

1. Estimate final Lagrange multipliers using Eq. (18), yielding $\lambda_1^*, \lambda_2^*, \dots, \lambda_p^*$.
2. Set $\lambda_i^0 = \lambda_i^*$, for $i = 1, \dots, p$.
3. Set $k = 1$ and $g^0 = y$.
4. Solve the PDE in Eq. (15) numerically (using the local relaxation method described in Sec. 7.4) to yield g^k .
5. Does g^k satisfy the constraints?
6. If not, update Lagrange multipliers $\lambda_1 \dots \lambda_p$ according to

$$\lambda_i^{k+1} = \lambda_i^k - \alpha \int_{-1}^1 \int_0^\pi g^k(t, \theta) \Psi_i(t, \theta) dt d\theta. \quad (19)$$

Set $k \leftarrow k + 1$ and go to 4.

7. Otherwise, we are done and $\hat{g} = g^k$.

The convergence time of this algorithm is the product of the number of iterations and the time per iteration, where the time per iteration is determined by the size of the problem. In step 4, the time required grows as \sqrt{N} , where $N = n_d n_v$ is the total number of pixels in the restored sinogram (see Sec. 7.4 and Ref. 22). In step 5, the time grows linearly with the number of Lagrange multipliers used. The number of iterations that are required is determined largely by the accuracy of the initial Lagrange multipliers and the size of α , the constant appearing in the Lagrange multiplier update formula of Eq. (19). As discussed in Sec. 7.3, the final Lagrange multipliers can be estimated well at the outset only in certain circumstances, one of which is not well satisfied when one has only limited-angle data. Therefore, as the range of unavailable projections increases, the convergence time can be expected to grow. For rapid convergence of the Lagrange multipliers, α should be chosen to be large, yet not so large that the sequence will not converge. Bertsekas²³ describes the selection of α and relates this generic primal-dual method to the method of multipliers, about which a great deal of theory is known. In our experiments, the initial value of α is chosen empirically and is modified adaptively over the course of iteration if the algorithm begins to diverge.

4. RESULTS

In this section we present results of simulations that demonstrate the performance of the sinogram restoration algorithm. The object under consideration and its full noise-free sinogram are shown in Figs. 2(b) and 2(a), respectively. The object is a binary ellipse of eccentricity 0.9 oriented with its long axis at -45° from the positive x -axis and with the letters M I T removed from the interior. This object is displayed using an 81×81 pixel image, as are all of the reconstructed objects shown in this section; however, the projections are computed exactly from the underlying parameterized object primitives (ellipse, rectangles, and triangles). Its sinogram consists of $n_v = 60$ total projections, which corresponds to the number of columns in the sinogram,

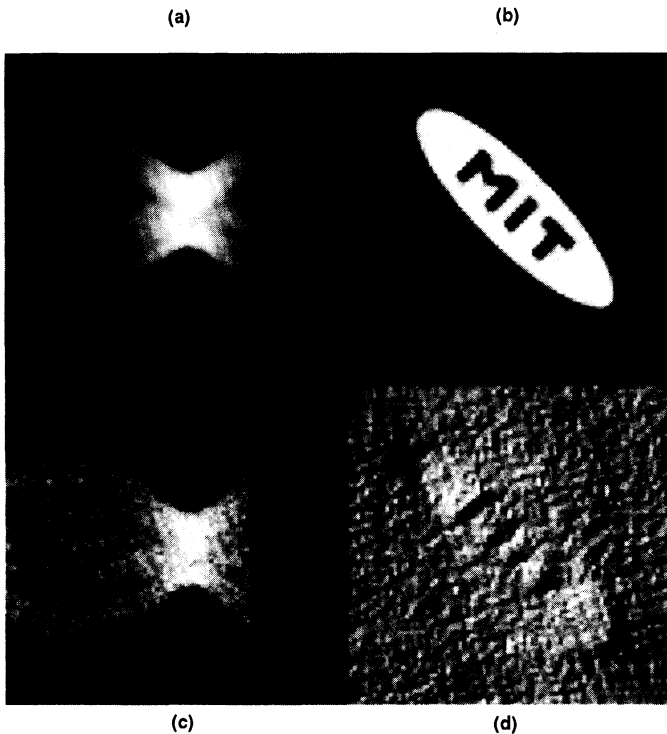


Fig. 2. The M.I.T. ellipse and its sinogram.

and $n_d = 81$ samples per projection, which gives the number of rows. For display purposes only, the range of angles in the displayed sinograms is $\pi/2$ for the projection on the left to $3\pi/2$ for the projection on the right.

To simulate noisy limited-angle measurements we first add noise, corresponding to a signal-to-noise ratio (SNR) of 10.0 dB, to the sinogram of Fig. 2(b), where

$$\text{SNR} = 10 \log \frac{\frac{\pi}{2} \frac{2}{n_v n_d} \sum_{j=1}^{n_v} \sum_{i=1}^{n_d} g^2(t_i, \theta_j)}{\sigma^2}, \quad (20)$$

yielding the noisy sinogram shown in Fig. 2(c). We then use only the left 40 (out of 60) projections as measurements, which is considered to be a severe test of a limited-angle tomography algorithm. A reconstruction using convolution backprojection assuming the missing projections to be identically zero is shown in Fig. 2(d).

To demonstrate the performance of the restoration algorithm we vary two smoothing parameters γ and β and the total number of constraints p that are used (using the ordering given in Sec. 7.2). The results of the simulations are shown in Figs. 3 through 5. Although the mass and center of mass are never explicitly enforced in the restoration method, it is also interesting to see how well these constraints are met. Therefore, Fig. 5 shows plots of the mass and center of mass of each projection as a function of the angle index for the four results appearing in Figs. 3 and 4. The correct values are $\mu = 1.0$ and $c(\theta) = 0.0$.

The sinogram shown in Fig. 3(a) and its reconstruction using CBP shown in Fig. 4(a) are the result of using the restoration algorithm with $\gamma = 0.0005$, $\beta = 0.01$ and $p = 0$. These values correspond to an amount of vertical smoothing that we found to yield good results in previous research,⁵ a small amount of horizontal smoothing, and no constraints. The mass and center

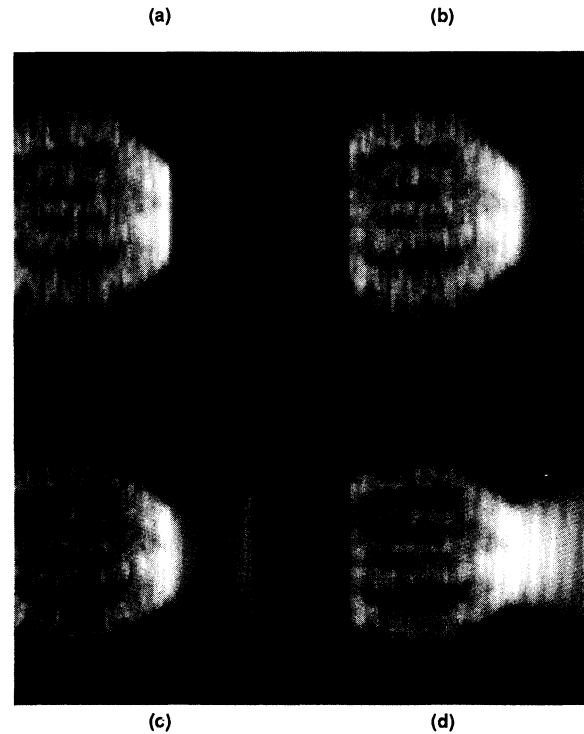


Fig. 3. Four restored sinograms: (a) $\beta = 0.01$, $\gamma = 0.0005$, and $p = 0$; (b) $\beta = 0.01$, $\gamma = 0.005$, and $p = 0$; (c) $\beta = 0.01$, $\gamma = 0.005$, and $p = 2$; and (d) $\beta = 0.01$, $\gamma = 0.05$, and $p = 22$.

of mass for the sinogram of Fig. 3(a) are shown using the dotted lines in Fig. 5. The result is an improvement over the raw CBP reconstruction of Fig. 2(d), and this is entirely due to noise smoothing effects since no constraints have been employed. It should be noted that the thin vertical stripe appearing at the right side of Fig. 3(a) is not an artifact; it is the result of a small amount of horizontal smoothing together with the boundary condition that ties the left and right sinogram boundaries together.

The sinogram shown in Fig. 3(b), its reconstruction in Fig. 4(b), and the dashed dotted curves in Fig. 5 correspond to the values $\gamma = 0.005$, $\beta = 0.01$, and $p = 0$. We notice from Fig. 5 that both the mass and center of mass move closer to their correct values in the second experiment and that this is due entirely to an increase in horizontal smoothing since no constraints were added. This increased horizontal smoothing effect is seen in the restored sinogram as an increased overall brightness in the region in which there are no observed projections. But one can also see that in the center of this range the sinogram is dark, implying that the mass constraint is not being met there.

The sinogram shown in Fig. 3(c), its reconstruction in Fig. 4(c), and the dashed curves in Fig. 5 correspond to the values $\gamma = 0.005$, $\beta = 0.01$, and $p = 2$. Comparing these results with those of Figs. 3(b) and 4(b) and their corresponding curves in Fig. 5 reveals that the addition of two constraints $p = 0$ and $p = 1$ causes the mass to move much closer to its correct value. The center of mass, however, remains completely unchanged. In the restored sinogram, the addition of these two constraints has the effect of dramatically increasing the brightness over the range of missing data, which corresponds to the improvement in meeting the mass constraint.

Finally, the sinogram shown in Fig. 3(d), its reconstruction in Fig. 4(d), and the solid curves in Fig. 5 correspond to the

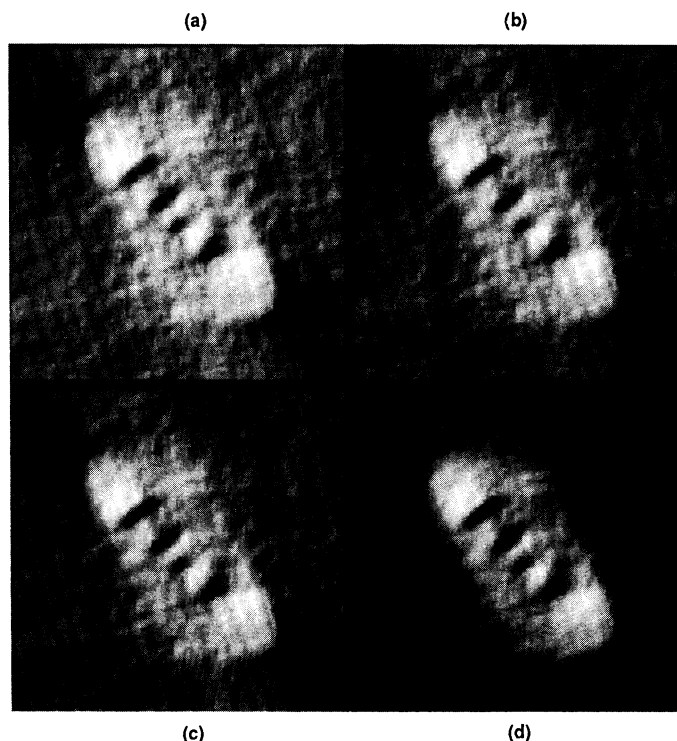


Fig. 4. Objects reconstructed from corresponding sinograms in Fig. 3.

values $\gamma = 0.05$, $\beta = 0.01$, and $p = 22$. This result constitutes a major change in the input parameters to the algorithm over those used in previous experiments. Here, we increased the horizontal smoothing coefficient γ to the value that we found to produce good results in Ref. 5. At the same time we increased the number of constraints to 22. The result is a sinogram and reconstruction that are noticeably better than the other results in this series and also better than the corresponding result in Ref. 5. As shown in Fig. 5, the mass and center of mass constraints are most closely met in this result. Also, one point that we observed in other simulation studies is that there are no noticeable improvements in the reconstructions for $p > 22$.

5. DISCUSSION

We have developed a projection-space reconstruction method for noisy and limited-angle tomography. The algorithm uses consistency, noise statistics, and smoothness to restore a complete sinogram, which is then used to reconstruct an object via convolution backprojection. The simulation results show that incorporation of smoothing and consistency conditions lead to improvements in the reconstructions. These reconstructions are also better than comparable experiments appearing in Ref. 5, in which only the mass and center of mass consistency was used.

It is useful to note that the variational formulation, on which the restoration algorithm is based, is analogous to maximizing an a posteriori probability, given a prior probability (on sinograms) described by a certain Markov random field (MRF) (see Refs. 5 and 6). In fact, the discrete solution found by the primal-dual method described in Sec. 4 exactly solves this MAP problem.⁵ Formulating the problem on the continuum, however, simplifies some of the development, for example, that which

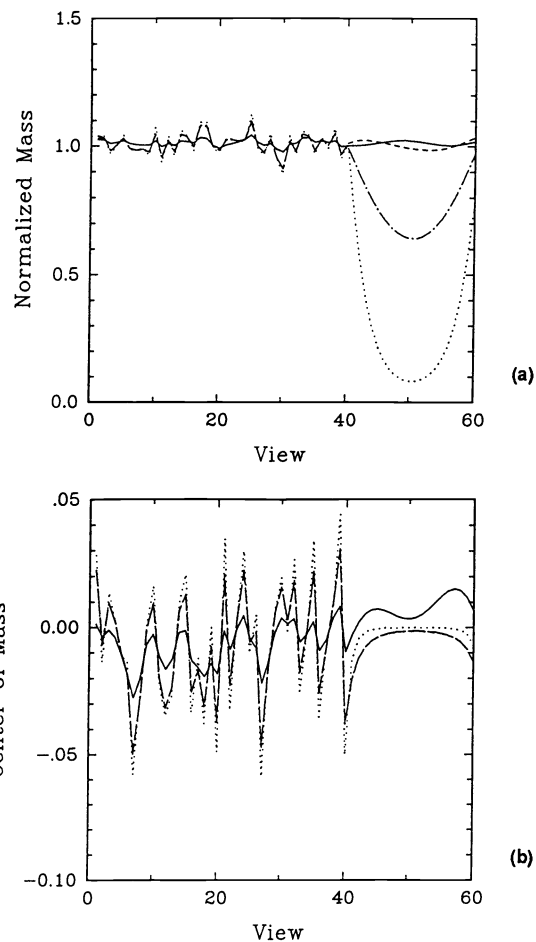


Fig. 5. (a) Mass of each restored projection and (b) center of mass of each restored projection.

led to the initial Lagrange multiplier estimates. Potentially, one can also exploit this relationship by using some of the new MRF parameter estimation procedures that have begun appearing in the literature. This would allow simultaneous estimation of the smoothing parameters β and γ , rather than having to fix these a priori. Cross validation is another method appearing in the literature for parameter estimation problems of this type. The determination of model parameter values, both a priori and simultaneously with restoration, is a subject of further research.

Another important consideration is parallelization. Although the algorithm was implemented on a serial computer, it should be noted that the primal phase (numerical solution of the PDE) can be implemented very efficiently in parallel, on a massively parallel architecture. Also, the dual phase may be implemented very rapidly on a vector processor since the central operation is an inner product. Implementation issues for parallel and vector architectures is also a subject of further research.

6. ACKNOWLEDGMENTS

This research was supported by National Science Foundation grant ECS-87-00903 and U.S. Army Research Office grant DAAL03-86-K-0171. In addition, the work of the first author was partially supported by a U.S. Army Research Office Fellowship.

7. APPENDIXES

7.1. Derivation of equilibrium PDE

The statement of the variational problem (V) appears in Eqs. (9), (11), and (14). In this appendix, we outline the steps required to show that $g(t, \theta)$ solves (V) if it satisfies the PDE given in Eq. (15) and with the additional boundary condition given in Eq. (16). In this section the notations g_t and g_{tt} stand for the first and second partial derivatives of $g(t, \theta)$ with respect to t , respectively, and g_θ and $g_{\theta\theta}$ stand for the first and second partial derivatives of $g(t, \theta)$ with respect to θ , respectively.

The problem is to find g that minimizes

$$I = \iint_{\mathfrak{y}} F(t, \theta, g, g_t, g_\theta) dt d\theta \quad , \quad (21)$$

where

$$F(t, \theta, g, g_t, g_\theta) = \beta g_t^2 + \gamma g_\theta^2 + \frac{1}{2\sigma^2} \chi r (y - g)^2 \quad , \quad (22)$$

subject to the stated constraints and boundary conditions. Following Ref. 21, we define

$$\tilde{J}_i = \lambda_i \iint_{\mathfrak{y}} g \Psi_i dt d\theta = 0 \quad , \quad i = 1, \dots, p \quad , \quad (23)$$

and minimize (unconstrained)

$$\tilde{I} = I + \sum_i^p \tilde{J}_i = \iint_{\mathfrak{y}} \tilde{F}(t, \theta, g, g_t, g_\theta) dt d\theta \quad . \quad (24)$$

We now introduce $p+1$ admissible test functions $v_1(t, \theta) \dots v_{p+1}(t, \theta)$ and form the $(p+1)$ -parameter family of comparison functions as

$$p(t, \theta) = g(t, \theta) + \sum_i^{p+1} \varepsilon_i v_i(t, \theta) \quad . \quad (25)$$

Then, minimizing

$$\tilde{I}(\varepsilon_1, \dots, \varepsilon_{p+1}) = \iint_{\mathfrak{y}} \tilde{F}(t, \theta, p, p_t, p_\theta) dt d\theta \quad (26)$$

with respect to the $(p+1)$ ε 's gives the necessary conditions

$$\left. \frac{\partial \tilde{I}}{\partial \varepsilon_i} \right|_{\varepsilon_i=0} \quad i = 1, \dots, p+1 \quad . \quad (27)$$

Taking the derivatives in Eq. (27), expanding terms, and using the divergence theorem leads to the formal statement of the necessary conditions:

$$\begin{aligned} \left. \frac{\partial \tilde{I}}{\partial \varepsilon_i} \right|_{\varepsilon_i=0} &= \iint_{\mathfrak{y}} \frac{\partial \tilde{F}}{\partial g} v_i - \frac{\partial}{\partial t} \left(\frac{\partial \tilde{F}}{\partial g_t} \right) v_i - \frac{\partial}{\partial \theta} \left(\frac{\partial \tilde{F}}{\partial g_\theta} \right) v_i dt d\theta \\ &+ \int_{\partial \mathfrak{y}} \left(\frac{\partial \tilde{F}}{\partial g_t} n_t + \frac{\partial \tilde{F}}{\partial g_\theta} n_\theta \right) v_i ds = 0 \quad , \quad i = 1, \dots, p+1 \quad , \quad (28) \end{aligned}$$

where n_t and n_θ are the coordinates of the outward pointing unit normal on the boundary $\partial \mathfrak{y}$. Both the Euler-Lagrange equation

$$\frac{\partial \tilde{F}}{\partial g} - \frac{\partial}{\partial t} \left(\frac{\partial \tilde{F}}{\partial g_t} \right) - \frac{\partial}{\partial \theta} \left(\frac{\partial \tilde{F}}{\partial g_\theta} \right) = 0 \quad (29)$$

and the integrated boundary condition

$$\int_{\partial \mathfrak{y}} \left(\frac{\partial \tilde{F}}{\partial g_t} n_t + \frac{\partial \tilde{F}}{\partial g_\theta} n_\theta \right) v_i ds = 0 \quad , \quad i = 1, \dots, p \quad (30)$$

follow from this result.

Equations (29) and (30) are formal statements of the PDE and new boundary condition, respectively, that we seek. To get the PDE, we simply compute the derivatives of F as follows:

$$\begin{aligned} \frac{\partial \tilde{F}}{\partial g} &= -\frac{1}{\sigma^2} \chi r (y - g) + \sum_{i=1}^p \lambda_i \quad , \\ \frac{\partial \tilde{F}}{\partial g_t} &= 2\beta g_t \quad , \\ \frac{\partial}{\partial t} \left(\frac{\partial \tilde{F}}{\partial g_t} \right) &= 2\beta g_{tt} \quad , \\ \frac{\partial \tilde{F}}{\partial g_\theta} &= 2\gamma g_\theta \quad , \\ \frac{\partial}{\partial \theta} \left(\frac{\partial \tilde{F}}{\partial g_\theta} \right) &= 2\gamma g_{\theta\theta} \quad , \end{aligned} \quad (31)$$

which gives the PDE of Eq. (15) except for the infinite sum. However, for any finite number of constraints p , the nature of the variational solution does not change. As p grows to infinity, so does the upper limit of the summation of terms appearing in Eq. (31). Therefore, in the limit, the summation becomes an infinite sum.

To see how the additional boundary condition arises, we first denote the boundary of \mathfrak{y} by ∂D and the four sides of \mathfrak{y} , starting on the right and proceeding counterclockwise, by ∂D_1 , ∂D_2 , ∂D_3 , and ∂D_4 . Since our original boundary conditions in Eq. (11) specify the value of g on ∂D_2 and ∂D_4 , our test functions v_i must be zero on ∂D_2 and ∂D_4 . However, g is only partially specified on ∂D_1 and ∂D_3 by the condition $g(t, 0) = g(-t, \pi)$. We now write Eq. (30) as

$$\int_{\partial D} (2\beta g n_t + 2\gamma g_\theta n_\theta) v_i ds = 0 \quad , \quad (32)$$

which becomes

$$\int_{\partial D_1} 2\beta g_t v_i ds + \int_{\partial D_3} 2\beta g_t v_i ds = 0 \quad (33)$$

since v_i is zero on ∂D_2 and ∂D_4 . Substituting the limits for t and the appropriate constant values for θ and dividing through by 2β , this becomes

$$\int_{-1}^1 g_t(t, \pi) v_i(t, \pi) dt - \int_{-1}^1 g_t(-t, 0) v_i(-t, 0) dt = 0 \quad . \quad (34)$$

Now, since v_i must satisfy the boundary conditions of Eq. (11), we have that $v_i(t, \pi) = v_i(-t, 0)$, which implies the desired additional boundary condition of Eq. (16).

A function $g(t, \theta)$ that satisfies the PDE of Eq. (15), the constraints, and boundary condition is simply a stationary function of (V). Because of the convex structure of the variational problem and the fact that the constraints are linear equalities, we can also conclude that a stationary function found in this manner is in fact a global minimum of the original variational problem (V).²⁴

7.2. Indexing the basis functions

The Lagrange multiplier λ_i corresponds to the constraint involving the basis function $\Psi_i(t, \theta) = P_k(t)S_{lm}(\theta)$, where i indexes the triplet (k, l, m) . We present in this appendix a method to order the infinite set of triple indices (k, l, m) so that for $i = 1, 2, \dots$, we have accounted for all of the Fourier coefficients in the constraints in Eq. (14).

There are three types of Fourier coefficients: (1) those that are free (unconstrained), (2) those that are constrained to be zero by the polynomial constraint, and (3) those that are trivially zero due to the fact that we enforce the periodicity condition of the 2-D Radon transform. This identification is independent of m , so for either $m = 1$ or $m = 2$ we may consider the classification of the Fourier coefficients by the value of k and l alone. Then, letting odd i correspond to $m = 1$ and even i correspond to $m = 2$, the integer

$$j = \begin{cases} \frac{(i+1)}{2}, & \text{for } i \text{ odd,} \\ \frac{i}{2}, & \text{for } i \text{ even,} \end{cases} \quad (35)$$

indexes the basis functions for either $m = 1$ or $m = 2$. Then, we determine k and l from j using

$$k = \begin{cases} 2(j - s^2 + s - 1), & \text{if } j \leq s^2, \\ 2(j - s^2 - 1) + 1, & \text{otherwise,} \end{cases} \quad (36)$$

$$l = \begin{cases} 2s, & \text{if } j \leq s^2, \\ 2s + 1, & \text{otherwise,} \end{cases} \quad (37)$$

where

$$s = [\sqrt{j} + 0.5]. \quad (38)$$

If one considers k and l to be the column and row index, respectively, of a matrix, then the above procedure indexes a checker-board of entries in the lower-left triangular region of the matrix. The column index increases while holding the row index constant until the entry reaches the diagonal, then the row index is incremented and the column index starts again at the left-most entry. This indexing scheme generates all of the free coefficients in the limit and at any finite stage includes the basis functions with the lowest frequency components.

7.3. Lagrange multiplier approximation

The integral expression for λ_j given in Eq. (17) consists of four separate additive integral terms. In this appendix, we consider

each term for possible simplification and approximation.

Term 1: The first term is trivially zero if $\chi_Y = 1$ on \mathcal{O} ; otherwise, we cannot reduce this term any further.

Term 2: The second term is approximately zero if β is small. To see this we integrate by parts in t twice and simplify, yielding

$$\int_0^\pi \int_{-1}^1 2\beta g_{tt} \Psi_j dt d\theta = \int_0^\pi \left(2\beta g_t \Psi_j \Big|_{-1}^1 + \int_{-1}^1 2\beta g \frac{\partial^2 \Psi_j}{\partial t^2} \right) d\theta, \quad (39)$$

where we have used the boundary condition $g(1, \theta) = g(-1, \theta) = 0$. The second term in the expression above is identically zero. To see this we substitute an explicit formula for $\partial^2 \Psi_j / \partial t^2$ into the expression to get for this term only

$$2\beta \int_0^\pi S_{ml}(\theta) \int_{-1}^1 g \frac{\partial^2 P_k(t)}{\partial t^2} dt d\theta = \beta \int_0^{2\pi} S_{ml}(\theta) \int_{-1}^1 g(t, \theta) \frac{\partial^2 P_k(t)}{\partial t^2} dt d\theta. \quad (40)$$

The equality results from use of (since $k+l$ is even) $2S_{ml}(\theta)P_k(t) = S_{ml}(\theta)P_k(t) + S_{ml}(\theta + \pi)P_k(-t)$ and simplification. Now by condition (c) of Theorem 1, we know that the integral over t must result in a polynomial in ω of order $\leq k-2$ [since the second derivative of $P_k(t)$ is a polynomial of order $k-2$]. Then, since $k < m$, we may conclude that the integral over θ is identically zero.

Hence, the second term in Eq. (17) may be written

$$\int_0^\pi \int_{-1}^1 2\beta \frac{\partial^2 g}{\partial t^2} \Psi_j dt d\theta = \int_0^\pi 2\beta \frac{\partial g}{\partial t} \Psi_j \Big|_{-1}^1 d\theta. \quad (41)$$

This term may or may not be nearly zero depending on the size of β and on the size of the support of the observations. For small β , however, we would expect this term to be nearly zero since $t = \pm 1$ represents the boundary of support for $f(x)$, and we would expect $f(x)$ to be approaching zero at its boundary.

Term 3: The third term in Eq. (17) is exactly zero. We see this by using the symmetries and periodicities of $S_{ml}(\theta)$, $g(t, \theta)$, and $P_k(t)$ to get

$$\int_0^\pi \int_{-1}^1 2\gamma \frac{\partial^2 g}{\partial \theta^2} \Psi_j dt d\theta = \gamma \int_0^{2\pi} S_{ml}(\theta) \frac{\partial^2}{\partial \theta^2} \int_{-1}^1 g(t, \theta) P_k(t) dt d\theta \quad (42)$$

for the third term. Then, the consistency theorem tells us that the integral over t is a polynomial in ω of degree $\leq k$, and since the second partial of such a polynomial does not change its degree, the integral over θ must be zero.

Term 4: The fourth term of Eq. (17) cannot be simplified.

Taking all of the simplifications together we have the following *exact* expression for λ_j :

$$\lambda_j = - \int_0^\pi \int_{-1}^1 \frac{2}{\sigma^2} \chi_{Yg} \Psi_j dt d\theta + \int_0^\pi 4\beta \frac{\partial g}{\partial t} \Psi_j \Big|_{-1}^1 d\theta + \int_0^\pi \int_{-1}^1 \frac{2}{\sigma^2} \chi_{Yy} \Psi_j dt d\theta. \quad (43)$$

Then, using the approximations derived above we have the following approximation for λ_j , which is valid when β is small, $f(x)$ is disappearing on its boundary, and χ_Y is 1 on \mathcal{O} :

$$\lambda_j \approx 2 \int_0^\pi \int_{-1}^1 \frac{1}{\sigma^2} \chi_{Yy} \Psi_j dt d\theta. \quad (44)$$

7.4. Local relaxation algorithm

The domain \mathcal{Q} is discretized evenly in t over the range $[-1, 1]$ using n_d samples and is discretized evenly in θ over the range $[0, \pi]$ using n_v samples. This describes a rectilinear grid with different vertical and horizontal sample spacing given by $\Delta_t = 2/n_d$ and $\Delta_\theta = \pi/n_v$, respectively. Given the usual approximations to the second partial derivatives of g ,

$$g_u \approx \frac{g_{i+1,j} - 2g_{i,j} + g_{i-1,j}}{\Delta_t^2}, \quad (45)$$

$$g_{\theta\theta} \approx \frac{g_{i,j+1} - 2g_{i,j} + g_{i,j-1}}{\Delta_\theta^2}, \quad (46)$$

we have

$$2\beta g_u + 2\gamma g_{\theta\theta} \approx \frac{2\beta}{\Delta_t^2}(g_{i+1,j} - 2g_{i,j} + g_{i-1,j}) + \frac{2\gamma}{\Delta_\theta^2}(g_{i,j+1} - 2g_{i,j} + g_{i,j-1}). \quad (47)$$

It is convenient to define new constants, $\hat{\beta}$ and $\hat{\gamma}$, as

$$\hat{\beta} = \frac{\beta}{\Delta_t^2}, \quad (48)$$

$$\hat{\gamma} = \frac{\gamma}{\Delta_\theta^2}. \quad (49)$$

Then the PDE of Eq. (15) may be approximated at an interior point by the finite difference equation²²

$$d_{i,j}g_{i,j} - r_{i,j}g_{i+1,j} - l_{i,j}g_{i-1,j} - t_{i,j}g_{i,j+1} - b_{i,j}g_{i,j-1} = s_{i,j}, \quad (50)$$

where

$$l_{i,j} = 2\hat{\beta}, \quad r_{i,j} = 2\hat{\beta}, \quad b_{i,j} = 2\hat{\gamma}, \quad t_{i,j} = 2\hat{\gamma},$$

$$d_{i,j} = 4\hat{\beta} + 4\hat{\gamma} + \frac{1}{\sigma^2} \chi_Y \Big|_{(i,\theta)}, \quad (51)$$

$$s_{i,j} = \left(\frac{1}{\sigma^2} \chi_{Y^2} - \frac{1}{2\sigma^2} \int_{-1}^1 \chi_Y y dt + \frac{m}{2\sigma^2} \chi_Y - \frac{3t}{2\sigma^2} \int_{-1}^1 t \chi_Y y dt \right) \Big|_{(i,\theta)}.$$

Equation (50) is also valid for boundary points when the boundary conditions in Eqs. (11) and (16) are taken into account.

Several traditional methods (cf. Ref. 25) including Jacobi, simultaneous over-relaxation, and Chebyshev semi-iterative relaxation methods may be employed to solve the set of equations in Eq. (50). We have chosen to implement a relatively new method credited to Kuo, Levy, and Musicus,²² which has been shown to have very favorable convergence properties and is relatively easy to implement. This method, in addition, has been shown to be ideally suited for parallel implementation. Our implementation of Kuo's local relaxation algorithm follows Ref. 22 closely.

We assume the PDE to be of the form

$$-p \frac{\partial^2 u}{\partial x_1^2} - q \frac{\partial^2 u}{\partial x_2^2} + \zeta(x_1, x_2)u = f(x_1, x_2), \quad (52)$$

where $(x_1, x_2) \in [0, 1] \times [0, 1]$, and we assume that it satisfies the conditions given in Ref. 22. Then the PDE is approximated by the five-point stencil given by Eq. (50). Each grid point is assigned a color, either red or black, according to an alternating pattern as on a checkerboard. Then the local relaxation procedure can be written as

red points ($i + j$ is even):

$$u_{i,j}^{(n+1)} = (1 - \omega_{i,j})u_{i,j}^{(n)} + \omega_{i,j}d_{i,j}^{-1} (lu_{i-1,j}^{(n)} + ru_{i+1,j}^{(n)} + bu_{i,j-1}^{(n)} + tu_{i,j+1}^{(n)} + s_{i,j}), \quad (53)$$

black points ($i + j$ is odd):

$$u_{i,j}^{(n+1)} = (1 - \omega_{i,j})u_{i,j}^{(n)} + \omega_{i,j}d_{i,j}^{-1} (lu_{i-1,j}^{(n+1)} + ru_{i+1,j}^{(n+1)} + bu_{i,j-1}^{(n+1)} + tu_{i,j+1}^{(n+1)} + s_{i,j}), \quad (54)$$

where $\omega_{i,j}$ is called the *local relaxation parameter* and is given by

$$\omega_{i,j} = \frac{2}{1 + \sqrt{1 - \rho_{i,j}^2}}, \quad (55)$$

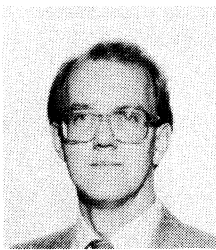
where

$$\rho_{i,j} = \frac{2}{d_{i,j}} \left(2\hat{\beta} \cos \frac{\pi}{n_v + 1} + 2\hat{\gamma} \cos \frac{\pi}{n_d + 1} \right). \quad (56)$$

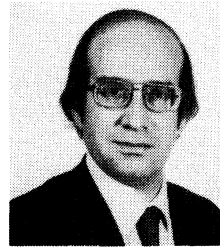
8. REFERENCES

1. D. Ludwig, "The Radon transform on Euclidean space," *Commun. Pure Appl. Math.* 19, 49–81 (1966).
2. S. Helgason, *The Radon Transform*, Birkhauser, Boston, Mass. (1980).
3. J. L. Prince and A. S. Willsky, "Reconstructing convex sets from support line measurements," *IEEE Trans. Pat. Anal. Mach. Intell.* 12(4), 377–389 (1990).
4. J. L. Prince and A. S. Willsky, "Reconstructing convex sets using prior geometric information," *CVGIP: Graphical Models and Image Processing*, in review (1989).
5. J. L. Prince and A. S. Willsky, "A geometric projection-space reconstruction algorithm," *Linear Algebra and Its Applications* 130, 151–191 (1990).
6. J. L. Prince "Geometric model-based estimation from projections," Ph.D. thesis, Massachusetts Inst. of Technology (1988).
7. A. K. Louis and F. Natterer, "Mathematical problems of computerized tomography," *Proc. IEEE* 71, 379–389 (1983).
8. K. T. Smith, D. C. Solmon, and S. L. Wagner, "Practical and mathematical aspects of the problem of reconstructing objects from radiographs," *Bull. AMS* 83, 1227–1270 (1977).
9. G. T. Herman, *Image Reconstruction from Projections*, Academic Press, New York (1980).
10. M. Ein-Gal, "The shadow transformation: an approach to cross-sectional imaging," Ph.D. thesis, Stanford Univ. (1974).
11. A. Peres, "Tomographic reconstruction from limited angular data," *J. Computer Assisted Tomography* 3(6), 800–803 (1979).
12. A. K. Louis, "Picture reconstruction from projections in restricted range," *Math. Meth. in the Appl. Sci.* 2, 209–220 (1980).
13. T. Saito and H. Kudo, "Tomographic image reconstruction from discretely viewed projections," preprint (1987).
14. J. H. Kim, K. Y. Kwak, and S. B. Park, "Iterative reconstruction-reprojection in projection space," *Proc. IEEE* 73, 1140–1141 (1985).
15. J. H. Kim, K. Y. Kwak, S. B. Park, and Z. H. Cho, "Projection space iteration reconstruction-reprojection," *IEEE Trans. Med. Imag.* MI-4, 139–143 (1985).
16. M. I. Sezan and H. Stark, "Tomographic image reconstruction from incomplete view data by convex projections and direct Fourier inversion," *IEEE Trans. Med. Imag.* MI-3(2), 91–98 (1984).
17. B. P. Medoff, "Image reconstruction from limited data: theory and applications in computerized tomography," in *Image Recovery: Theory and Application*, H. Stark, ed., pp. 321–368, Academic Press, Orlando, Fla. (1987).

18. M. Ravichandran and F. C. Gouldin, "Reconstruction of smooth distributions from a limited number of projections," *Appl. Opt.* 27, 4084-4097 (1988).
19. M. H. Buonocore, "Fast minimum variance estimators for limited angle computed tomography image reconstruction," Ph.D. thesis, Stanford Univ. (1981).
20. T. Kailath, *Lectures on Wiener and Kalman Filtering*, Springer-Verlag, New York (1981).
21. F. B. Hildebrand, *Methods of Applied Mathematics*, Prentice-Hall, Englewood Cliffs, N.J. (1965).
22. C. J. Kuo, B. C. Levy, and B. R. Musicus, "A local relaxation method for solving elliptic PDE's on mesh-connected arrays," *SIAM J. Sci. Stat. Comput.* 8(4), 550-573 (1987).
23. D. P. Bertsekas, *Constrained Optimization and Lagrange Multiplier Methods*, Academic Press, New York (1982).
24. D. G. Luenberger, *Optimization by Vector Space Methods*, Wiley, New York (1969).
25. R. S. Varga, *Matrix Iterative Analysis*, Prentice-Hall, Englewood Cliffs, N.J. (1962).



Jerry L. Prince received a BS degree from the University of Connecticut in 1979 and SM, EE, and Ph.D. degrees in 1982, 1986, and 1988, respectively, from the Massachusetts Institute of Technology, all in electrical engineering and computer science. From 1982 to 1983 Dr. Prince was employed at the Brigham and Women's Hospital in Boston, where he developed instrumentation and reconstruction algorithms for ultrasonic imaging in medicine. In 1988 he was a member of the technical staff at The Analytic Sciences Corporation (TASC) in Reading, Mass., where he contributed to the design of an automated vision system for synthetic aperture radar imaging. He joined the faculty at the Johns Hopkins University in 1989, where he is currently an assistant professor in the Department of Electrical and Computer Engineering and holds a joint appointment in the Department of Radiology. Dr. Prince is a member of IEEE, Sigma Xi, Tau Beta Pi, Eta Kappa Nu, and Phi Kappa Phi. His current research interests are in multidimensional signal processing, medical imaging, computational geometry, and computer vision.



Alan S. Willsky received the SB and Ph.D. degrees from the Massachusetts Institute of Technology in 1969 and 1973, respectively. From 1969 to 1973 he held a Fannie and John Hertz Foundation Fellowship. He joined the M.I.T. faculty in 1973; his present position is professor of electrical engineering. From 1974 to 1981 Dr. Willsky served as assistant director of the M.I.T. Laboratory for Information and Decision Systems. He is also a founder and member of the board of directors of

Alphatech, Inc. In 1975 he received the Donald P. Eckman Award from the American Automatic Control Council. Dr. Willsky has held visiting positions at Imperial College, London; L'Université de Paris-Sud; and the Institut de Recherche en Informatique et Systèmes Aléatoires in Rennes, France. He is editor of the M.I.T. Press series on signal processing, optimization, and control; was program chairman for the 17th IEEE Conference on Decision and Control; has been an associate editor of several journals, including the *IEEE Transactions on Automatic Control*; has served as a member of the Board of Governors and vice president for technical affairs of the IEEE Control Systems Society; and was program chairman for the 1981 Bilateral Seminar on Control Systems, held in China. In addition, Dr. Willsky gave the opening plenary lecture at the 20th IEEE Conference on Decision and Control and in 1988 was made a distinguished member of the IEEE Control Systems Society. Dr. Willsky is the author of the research monograph *Digital Signal Processing and Control and Estimation Theory* and is coauthor of the undergraduate text *Signals and Systems*. He was awarded the 1979 Alfred Noble Prize by the American Society of Civil Engineers and the 1980 Browder J. Thompson Memorial Prize Award by the IEEE for a paper excerpted from his monograph. Dr. Willsky's present research interests deal with problems involving multidimensional and multiresolution estimation and imaging, discrete-event systems, and the asymptotic analysis of control and estimation systems.